THE JOURNAL OF PHYSICAL CHEMISTRY A

 VOLUME 109, NUMBER 27, JULY 14, 2005

ARTICLES

Excited-State Proton Transfer: Indication of Three Steps in the Dissociation and Recombination Process

Pavel Leiderman, Liat Genosar, and Dan Huppert*

Raymond and Beverly Sackler Faculty of Exact Sciences, School of Chemistry, Tel Aviv University, Tel Aviv 69978, Israel

Received: January 4, 2005; In Final Form: May 10, 2005

A femtosecond pump−probe, with ∼150 fs resolution, as well as time-correlated single photon counting with ∼10 ps resolution techniques are used to probe the excited-state intermolecular proton transfer from HPTS to water. The pump−probe signal consists of two ultrafast components (∼0.8 and 3 ps) that precede the relatively slow (∼100 ps) component. From a comparative study of the excited acid properties in water and methanol and of its conjugate base in basic solution of water, we propose a modified mechanism for the ESPT consisting of two reactive steps followed by a diffusive step. In the first, fast, step the photoacid dissociates at about 10 ps to form a contact ion pair $RO^-{}^*\cdots H_3O^+$. The contact ion pair recombines efficiently to re-form the photoacid with a recombination rate constant twice as large as the dissociation rate constant. The first-step equilibrium constant value is about 0.5 and thus, at short times, <10 ps, only ∼30% of the excited photoacid molecules are in the form of the conjugated base−proton contact ion pair. In the second, slower, step, of about 100 ps, the proton is separated by at least one water molecule from the conjugate base $RO^-{}^*$. The separated proton and the conjugated base can recombine geminately as described by our previous diffusion-assisted model. The new two-step reactive model predicts that the population of the ROH form of HPTS will decrease with two time constants and the RO^- population will increase by the same time constants. The proposed model fits the experimental data of this study as well as previous published experimental data.

Introduction

Proton-transfer reactions are among the most common and important chemical and biological processes.[1−4] Over the last two decades, intermolecular proton transfer in the excited state (ESPT), in aqueous solutions and other protic media, has been the subject of intensive theoretical and experimental investigation as they provide valuable information about the mechanism and nature of acid−base reactions.[5−11]

To initiate these reactions, protic solvent solutions of suitable organic molecules are irradiated by short (femtosecond−picosecond) laser pulses.[12−14] Consequently, the excited-state molecules dissociate very rapidly by transferring a proton to a nearby solvent molecule.

Over the past 15 years we used a model for an intermolecular ESPT process that accounts for various observable experimental data. In this model, the overall dissociation process can be subdivided into the two consecutive steps of reaction and diffusion. In the reactive stage, a rapid short-range charge separation occurs, and a solvent-stabilized ion pair is formed. This is followed by a diffusive stage, when the two ions withdraw from each other due to their thermal random motion. The reverse process is geminate recombination (neutralization)

* Corresponding author. E-mail: huppert@tulip.tau.ac.il. Fax/phone: 972-3-6407012.

10.1021/jp050037b CCC: $30.25
Published on Web 06/17/2005

of the two separated ions either by the direct collapse of the ion pair, or following a geminate reencounter of the solvated "free" ions. Scheme 1 shows the model schematically.[15−22]

SCHEME 1

$$\mathrm{ROH}^* \underset{k_r}{\overset{k_{PT}}{\rightleftharpoons}} [\mathrm{RO}^-{}^*\cdots\mathrm{H}^+]_{(r=a)} \overset{\mathrm{DSE}}{\rightleftharpoons} \mathrm{RO}^-{}^* + \mathrm{H}^+$$

The first step is described by back-reaction boundary conditions k_{PT} and k_r. This is followed by a diffusional second step, in which the hydrated proton is removed from the parent molecule solvation shell. In the continuous diffusion approach, one describes this dissociation reaction second step by a spherically symmetric three-dimensional diffusion equation, the Debye−Smoluchowski equation (DSE).[23,24] The boundary conditions at $r = a$ are those of the back reaction.[16,17] k_{PT} and k_r are the "intrinsic" dissociation and recombination rate constants at the contact sphere radius a.

Quantitative agreement was obtained between theory and experiment, and as a result, it was possible to make a closer study of the ESPT process itself, and also the dynamic and static properties of the solvent.

8-Hydroxypyrene-1,3,6-trisulfonate (HPTS or pyranine) is a photoacid that is commonly used in studying the ESPT process. The RO^- form is quadruply negatively charged. Thus, the reversible geminate recombination process is strongly enhanced relative to a singly charged photoacid like 2-naphthol. We have studied HPTS ESPT for many years.[22,25−27] Using the TCSPC technique enabled us to determine the rate of proton transfer to water to be $(100\ \mathrm{ps})^{-1}$. The proton-transfer rate could be determined either by the initial decay time of the time-resolved fluorescence of the protonated form (ROH) measured at 440 nm or by the slow rise-time of the emission of the deprotonated species (RO^-).

Prayer et al.[10] and Tran-Thi and co-workers[11] used both femtosecond fluorescence up-conversion[10] and pump−probe spectroscopies[11] to probe the excited-state proton transfer (PT) from HPTS to water. They found that the process involves two ultrafast steps (300 fs and 2.5 ps) that precede the relatively slow (87 ps) proton-transfer step. They concluded that the excited-state proton-transfer reaction from HPTS to water is a much more complex process than previously reported in the literature. The first could be assigned to a fast solvation process within the LE state of the acid reached in absorption from the ground state. In the second step, LE relaxes within 2.5 ps to a second, somewhat mysterious, intermediate species, which they tentatively assign to an electronic state displaying a CT character.

The acid ionization of HCl in water was theoretically studied by a combination of electronic structure calculations with ab initio molecular orbital methods and Monte Carlo computer simulations by Ando and Hynes.[28] They found that the mechanism involves two reactive steps: first, a nearly activationless motion in a solvent coordinate, which is adiabatically followed by the quantum proton to produce a contact ion pair $Cl^-{-}H_3O^+$, which is stabilized by ∼7 kcal/mol. The second step includes the motion in the solvent with a small activation barrier, as a second adiabatic proton-transfer stage that produces a solvent-separated ion pair from the contact ion pair in a nearly thermoneutral process. The motion of a neighboring water molecule to accommodate the change of the primary coordination number from 4 for H_2O to 3 for H_3O^+ of a proton-accepting water molecule-is indicated as a key feature in the necessary solvent reorganizations.

In our previous time-resolved emission studies of HPTS in water measured by TCSPC, the protonated form ROH decays exponentially at early times at about 100 ps. The RO^- fluorescence signal rise time showed that it consists of two components—a short one of <20 ps with amplitude of about 20% and a long component of about 100 ps that matches the decay time of the ROH signal. We interpreted for many years this observed short-time component as arising from a large overlap between the emissions of ROH and RO^-. We claim in this paper that the inconsistency in the TCSPC time-resolved emission signal of the ROH decay and complementary rise of RO^- arises from a missing reactive step in the proton-transfer reaction mechanism and from the limited time resolution of TCSPC technique. The missing reactive step is fast, 3 ps, and cannot be observed by the TCSPC technique.

Recently, Rini[9,29] et al. studied, by means of femtosecond pump−probe IR spectroscopy, the acid−base reaction of HPTS with acetate ions in a D_2O solution. A relatively large fraction of HPTS−acetate contact complexes already exists in the ground state in high concentrations of acetate ions (>2 M). The rate of excited-state proton transfer from HPTS to acetate in the contact complex was faster than 150 fs, the time resolution of their experimental response. Rini et al.[9,29] proposed an extended three-state Eigen-Weller[3,4] model to explain the overall observations of the acid−base experiments, including the slow components of the pump−probe experiments. In the first reaction stage, the acid and base form a ''loose" encounter complex where each species retains its water solvation shell. This stage is governed by diffusion and the encountered complex is described by the contact distance a. The second reaction stage occurs within the contact volume and is largely controlled by the solvent. The time scale for the second reaction stage time constant of 6 ps is governed by the solvent reorganization dynamics and is slightly faster than the Debye relaxation. This intermediate reaction stage is relatively slow compared with the final, inner sphere reaction stage of the proton transfer, which is faster than 150 fs.

In this study we measured, by time-resolved emission and absorption spectroscopies, the ESPT process from HPTS to water. We used the TCSPC and femtosecond pump−probe techniques. On the basis of our experimental data and the data presented in recent papers of Prayer et al.[10] and Tran-Thi et al.[11] and from model calculations made by Ando et al.,[28] we developed a new model for the intermolecular ESPT processes.

The new model extends our previous diffusion-assisted excited-state proton-transfer model to include an additional reactive step (see Schemes 1 and 2). The excited protonated acid ROH* dissociates first to a contact ion pair, consisting of an anion and a hydrogen bonded hydrated proton complex, which we designate H_3O^+. The contact ion pair $RO^-\cdots H_3O^+$ exhibits about the same spectroscopic signature as the RO^- emission band of the separated and solvated ion pair. Similar models for acid dissociation were suggested by Eigen[4] and Ando and Hynes.[28]

A simple and straightforward description of the modified ESPT model is given by Scheme 2,

SCHEME 2

$$\mathrm{ROH}^* + \mathrm{H_2O} \overset{\text{step one}}{\underset{k'_r}{\overset{k'_{PT}}{\rightleftharpoons}}} \underset{\text{contact ion pair}}{[\mathrm{RO}^-{}^*\cdots\mathrm{H_3O}^+]_{(r=a)}} \overset{\text{step two}}{\underset{k_r}{\overset{k_{PT}}{\rightleftharpoons}}}$$

$$\underset{\text{separated ion pair}}{[\mathrm{RO}^-{}^*{---}\mathrm{H_3O}^+]_{(r=a)}} \overset{\text{step three}}{\overset{\mathrm{DSE}}{\rightleftharpoons}} \mathrm{RO}^-{}^* + \mathrm{H_3O}^+$$

where R is an organic radical and $[RO^-\cdots H_3O^+]$ is the contact ion pair formed between the molecular anion RO^- and the proton H^+, separated by a short distance a'. k'_{PT} and k'_r are the forward and reverse rate constants of the first step, respectively. Our old model covers the second and the third steps. Details of our old model including the second reactive step and the diffusive part are given in a separate section.

Experimental Section

Time-resolved fluorescence was acquired using the time-correlated single-photon counting (TCSPC) technique, the method of choice when sensitivity, large dynamic range and low intensity illumination are important criteria in fluorescence decay measurements.

For excitation we used a cavity dumped Ti:sapphire femtosecond laser, Mira, Coherent, which provides short, 80 fs, pulses of variable repetition rate, operating at the SHG frequency, over the spectral range 380−400 nm and with the relatively low repetition rate of 500 kHz. The TCSPC detection system is based on a Hamamatsu 3809U, photomultiplier and Edinburgh Instruments TCC 900 computer module for TCSPC. The overall instrumental response was about 35 ps (fwhm). Measurements were taken at 10 nm spectral width. The excitation pulse energy was reduced by neutral density filters to about 1 pJ. We checked the sample's absorption prior to and after time-resolved measurements. We could not find noticeable changes in the absorption spectra due to sample irradiation.

For the pump−probe experiments reported, we used an amplified femtosecond Ti:sapphire laser system. In brief, laser pulses (50 fs duration, centered near 800 nm with pulse energy of ~600 μJ) at a 1 kHz repetition rate were generated by a Ti:sapphire-based oscillator (Coherent Mira seed) and amplified by a multipass Ti:sapphire amplifier (Odin Quantronix). Samples were excited by the second harmonic of the amplified laser (~400 nm). To obtain probe pulses, we generate a super continuum by focusing 1 μJ of either the 800 nm or a 400 nm (the second harmonic of 800 nm) pulse onto a 2 mm thick sapphire window. The continuum generated with the 400 nm beam provides a probe pulse in the region of 410−500 nm. The probe beam signal was measured by a combination of a chopper/lockin amplifier and computer averaging. Interference filters of 8 nm fwhm bandwidth at the proper wavelength were used in front of the probe beam detector, a silicon photodiode. The time-resolved pump−probe spectra were measured by a miniature diode-array spectrometer SM-240, (CVI) with about 2 nm resolution. Samples were placed in a rotating optical cell to avoid degradation.

Steady-state fluorescence spectra were taken using a FluoroMax (Jobin Yvon) spectrofluorometer.

The Old Reversible Diffusion-Influenced Two-Step Model of Pines, Huppert, and Agmon

The model is given schematically in Scheme 1. In the continuous diffusion approach, the photoacid dissociation reaction is described by the spherically symmetric diffusion equation (DSE)[30] in three dimensions.[16,27] The boundary conditions at $r = a$ are those of the back reaction (Scheme 1). k_{PT} and k_r are the "intrinsic" dissociation and recombination rate constants at the contact sphere radius, a. A detailed description of the model, as well as the fitting procedure, is given in the refs 16, 27, and 31.

The solution of the DSE is determined by several parameters:

(a) The unscreened Coulomb potential $V(r) = R_D/r$, which is governed by the Debye radius

$$R_D = \frac{|z_1 z_2| e^2}{\epsilon k_B T} \quad (1)$$

determined by the charges z_1 and z_2 of the proton and anion, the static dielectric constant ϵ of the solvent, and the absolute temperature T, where e is the electronic charge and k_B is the Boltzmann constant.

(b) The contact distance, a, which is the center-to-center distance of a separated ion pair. The motion is assumed diffusive for $r > a$.

(c) The relative anion−proton diffusion constant D, which is almost the same as the (very large) protic diffusion constant.[32,33]

(d) The initial separation of the proton after thermalization, r_0. Here we assume that r_0 is that of a bound proton, so that this parameter plays no role in our analysis.

(e) The intrinsic dissociation and recombination rate constants to and from contact designated k_{PT} and k_r, respectively.

Quantitative agreement was obtained between theory and experiment, and as a result, it was possible to make a closer study of the ESPT process itself, and also of the dynamic and static properties of the solvent.

The asymptotic expression (the long-time behavior) for the fluorescence of ROH* is given by[35]

$$[\mathrm{ROH}^*]\exp(t/\tau_f) \cong \frac{\pi}{2}a^2 \exp(R_D/a)\frac{k_r}{k_{PT}(\pi D)^{3/2}} t^{-d/2} \quad (2)$$

where τ_f is the excited-state lifetime of the deprotonated form RO^-, d is the dimensionality of the relevant problem, and all other symbols as previously defined. Equation 2 shows that the tail amplitude depends on several parameters but its time dependence is a power law of time that depends on the dimensionality of the problem. For 3 dimensions it assumes the power law of $t^{-3/2}$.

For the numerical fit, we used the user-friendly graphic program, SSDP (Ver. 2.63), of Krissinel and Agmon.[34] The comparison of the calculated signal with the experimental results involves several parameters. Usually, the adjustable parameters are the proton-transfer rate to the solvent, k_{PT}, and the geminate recombination rate, k_r. k_{PT} determines the initial slope of the decay curves: the larger k_{PT}, the faster the initial exponential drop. The intrinsic recombination rate constant, k_r, does not affect the behavior at $t \rightarrow 0$ but determines the magnitude of the long-time tail. The effect of increasing k_r is somewhat similar to decreasing D. It differs from the effect of changing R_D or a in the curvature of these plots. The parameters for the numerical solution of the DSE were taken from the literature.[36,37] The contact radius $a = 6$ Å is slightly larger than the molecule spherical gyration radius (4.5−5.5 Å) obtained from measurements of HPTS rotation times.[38] It probably accounts for at least one layer of water molecule around the HPTS anion.

Results

Figure 1a shows the time-resolved emission of HPTS in water ($4.5 \leq$ pH ≤ 5.5) using the TCSPC technique. The sample was excited near the peak of the ROH band at 394 nm. Figure 1a shows the emission of the protonated form, ROH*, in a water solution of pH $\sim 5 \pm 0.5$ measured at 435 nm, close to the peak emission at 432 nm. The solid curve is a fit using the SSDP program to solve the DSE with the appropriate initial

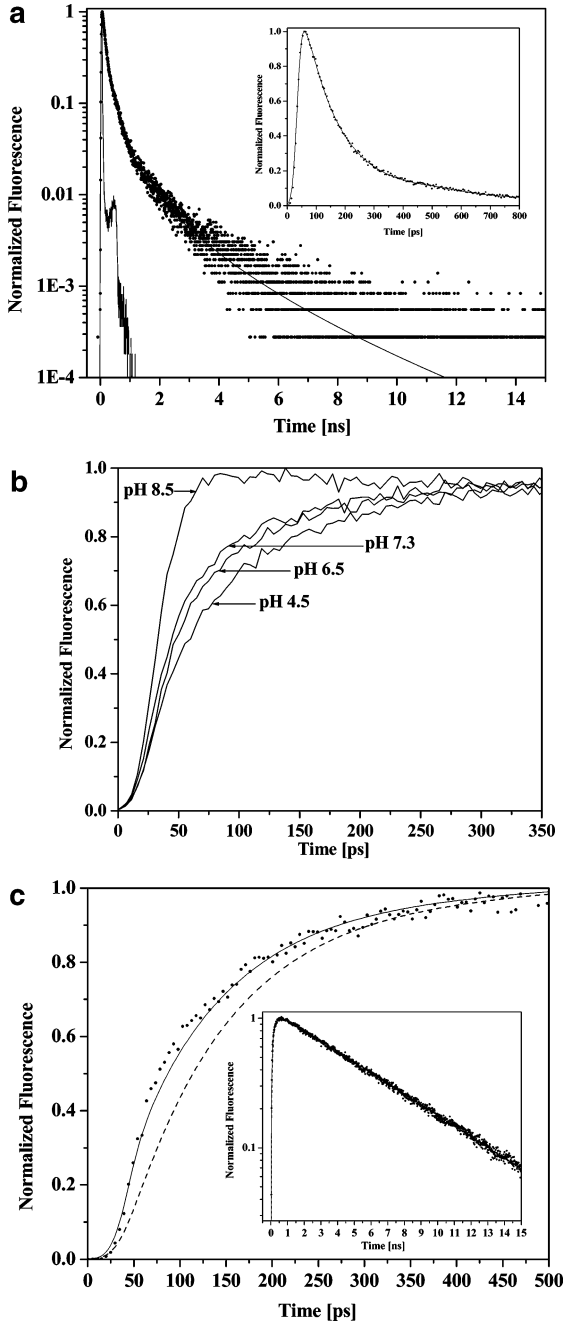

Figure 1. Time-resolved emission of HPTS in water at pH ~ 6 using the TCSPC technique. The sample was excited near the peak of the ROH band at 394 nm. (a) Emission of the protonated form ROH* was measured at 435 nm, close to the emission peak of 432 nm. The solid curve is a fit using the SSDP. The instrument response function is also shown in the figure. (b) Time-resolved emission of the RO^- of HPTS in aqueous solution of various pH in the range $4 < pH < 9$. (c) Time-resolved emission of the RO^- of HPTS in a solution of pH 5. The dashed line is a fit using the SSDP program with the parameters of Table 1 that were also used to fit the ROH signal shown in Figure 1a. The solid line is constructed by adding a fast-rise-time component with an amplitude of 0.22.

and boundary conditions. The parameters for the fit are given in Table 1. The instrument response function is also shown in the figure. The fwhm is 35 ps. Figure 1b shows the time-resolved emission of the RO^- band of various aqueous solutions at a deferent pH values in the range $4.15 \leq pH \leq 9$. As seen in the figure, the signal is independent of the pH, below pH 6. At a higher pH values, the amplitude of the fast component increases

TABLE 1: Kinetic Parameters for the Proton-Transfer Reaction of HPTS in Water Using the Diffusion-Assisted Geminate Recombination Model

	k_{PT} [10^9 s^{-1}]	k_r [10^9 Å s^{-1}]	R_D [Å]	D [cm^2 s^{-1}]	τ_{ROH} [ns^{-1}]	τ_{RO^-} [ns^{-1}]
HPTS/H_2O	8.8	5	28	0.0001	0.19	0.19

with increasing pH value. At pH 9 the signal solely arises from a direct excitation of the ground-state population of the RO^-(g).

Figure 1c shows the TCSPC time-resolved emission of the RO^- form of HPTS measured in pH ~ 5.5 solution when the solid line is a fit of the RO^- emission using the SSDP program with the parameters of Table 1 that were used to fit the ROH emission shown in Figure 1a. The fit is bad for short times and much better for longer times. The dashed line shows the fit when we use a large overlap between the ROH and RO^- signals. In the fit shown in the figure, we used amplitude of ~22% of the ROH band with amplitude of only 78% of the RO^- band.

Figure 2 shows the steady-state emission spectra of the HPTS-water ethanol mixture. The solution composition is designated on the right-hand side of the figure. The excitation wavelength, 394 nm, was the same as that used in the time-resolved emission shown in Figure 1. The points to note in the figure are as follows:

1. The bandwidths of both the ROH and the RO^- 510 nm band are about the same.

2. The ROH and RO^- emission peaks' height are about the same.

3. The isoemissive point is at about 480 nm.

4. The lifetime of both species is about the same, 5.4 ns in N_2 purged samples. The fluorescence quantum yield of the RO^- emission (when excited in basic solutions) is about 0.9.

5. The relative fluorescence intensity of the ROH band in neat ethanol at 520 nm, close to the peak of RO^- is $I^{ROH}_{f(520)}/I^{ROH}_{f(430)} \approx 4.5\%$. Most of our TCSPC RO^-* measurements were taken in water at 520 nm. A detailed procedure to estimate the overlap between ROH and RO^- emission in water solution at 520 nm is given in the Supporting Information. In water, we estimate that the fluorescence intensity ratio is larger and is about 11%.

6. The main conclusion drawn from Figure 2 and from the estimate of the fluorescence band overlap is that the computer fit of the data shown in Figure 1b of the RO^-, using a 22% overlap of ROH emission, is unjustified.

Pump−Probe Experiments. Figure 3a shows the pump-probe signal of HPTS in a water solution of pH ~ 5.5 at the selected wavelengths 510−600 nm (the signals are normalized

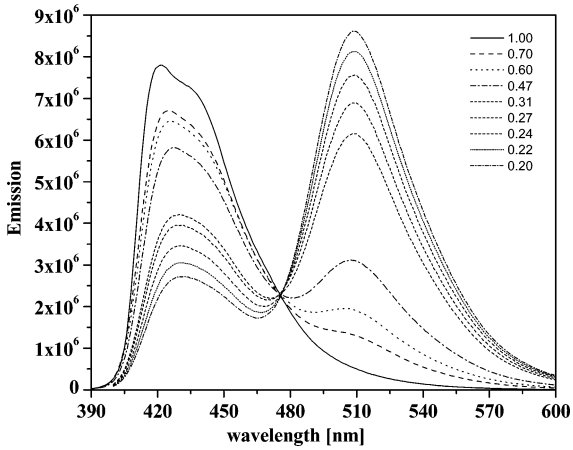

Figure 2. Steady-state emission spectra of the HPTS water−ethanol mixtures (mol fraction of EtOH). The excitation wavelength is 394 nm.

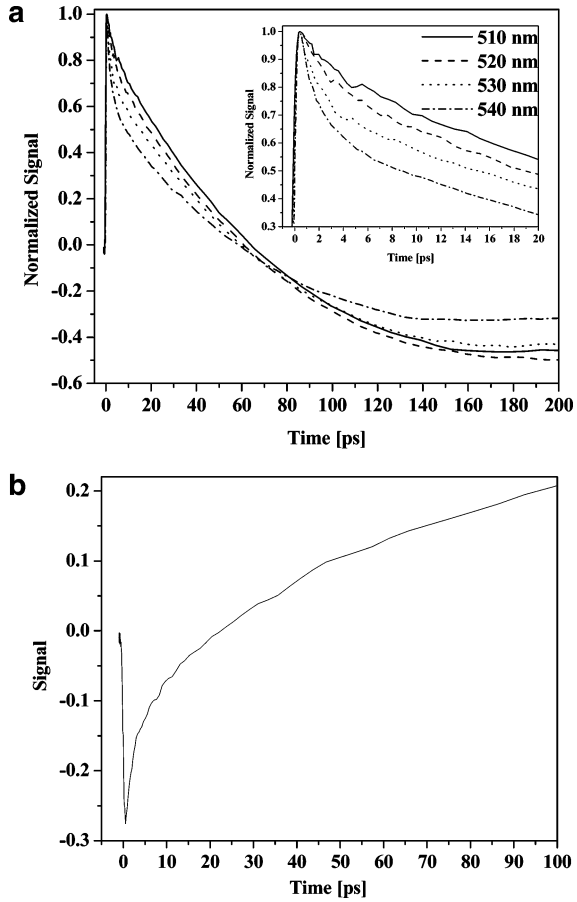

Figure 3. Pump−probe normalized signal of HPTS in a water solution of 5.5 < pH < 6.5: (a) at selected wavelengths between 510 and 540 nm; (b) at 430 nm.

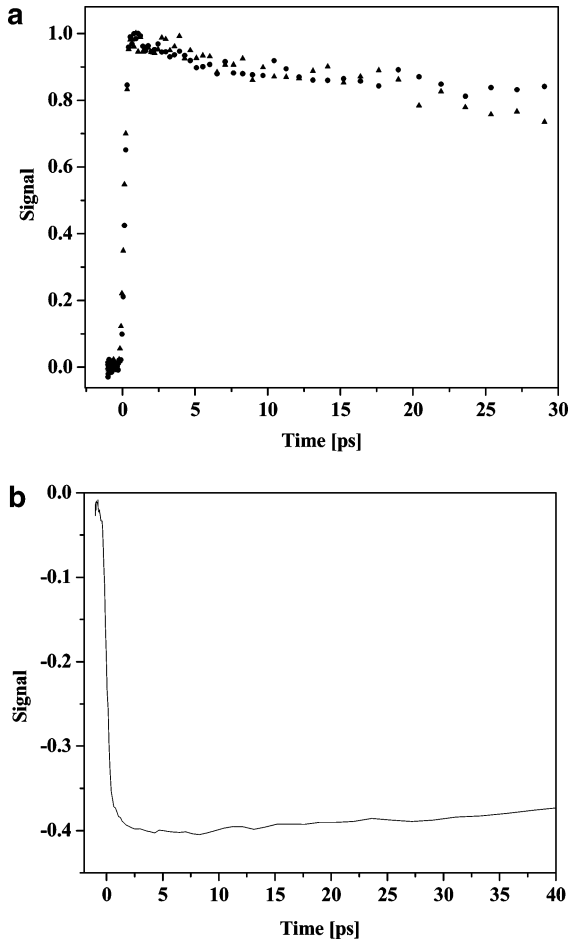

Figure 4. Pump−probe signal of HPTS in a methanol solution probed at selected wavelengths: (a) ●, 560 nm; ▲, 540 nm; (b) 430 nm.

to 1 at the peak intensity). The samples were excited by the SHG of the multipass amplified Ti:sapphire laser system at about 395 nm, close to the absorption band maximum (406 nm) of the protanated form of HPTS.

The pump−probe signal consists of three time components of ∼0.8, 3, and about 100 ps. The relative amplitude depends on the probe wavelength. At the wavelengths 520−580 nm, the pump−probe signal gets negative values at times longer than 60 ps. In general, the pump−probe signal of an HPTS−water solution at a particular wavelength is a superposition of both the excited-state absorption and stimulated emission to the ground state. The stimulated emission signal is displayed as a negative signal whereas the absorption appears as positive signal. The shape of the pump−probe signal is almost independent of the pump and probe intensities. The signal-to-noise value decreases as the pump intensity decreases. As seen in Figure 3, the amplitude of the shortest component is large for long wavelengths. The negative amplitude is larger for short wavelengths. Figure 3b shows the pump−probe signal of HPTS in aqueous solution of pH ∼ 5.5, excited at 395 nm and probed at 430 nm. The white light continuum was generated by focusing a 2 μJ 395 nm pulse on a 2 mm sapphire window. The probe at 430 nm, with a 15 nm fwhm, was shaped and filtered by a combination of colorglass filters. The signal at short time is negative, and at longer times, t > 20 ps is positive. The amplitude of the negative signal at $t \sim 0$ has about the same value as the positive signal at 100 ps. The negative signal arises from the stimulated emission of the ROH emission band, centered at about 434 nm. The positive signal arises from $S_1 \rightarrow S_2$ absorption of the RO^- form. The pump−probe signal of the ROH band shown in Figure 3b is inverted, but similar in shape to the signal probed at 540 nm, shown in Figure 3a. It consists of three time components: short, medium, and long.

Figure 4a shows the pump−probe signal of HPTS in a methanol solution at selected wavelengths in the spectral region 510−600 nm. As seen in the figure, the signal is positive with a very large amplitude of immediate rise time that follows the pump−probe cross-correlation signal of about 250 fs fwhm. Figure 4b shows the pump−probe signal of HPTS in methanol neutral solution, pumped at 395 nm, and probed at 430 nm. The signal intensity is constant in time and negative. This is a control experiment to the data shown in Figure 3b, in which the signal is time-dependent because proton transfer occurs in the excited state.

Figure 5 shows the pump−probe signal of HPTS in water at pH ∼ 10. In such a solution, the dominate form is the deprotonated HPTS: RO^-. The ground-state equilibrium of HPTS is pK = 7.7 approximately, and thus at pH ∼ 10, about 99% of the molecules are in the RO^- form in the ground state. As seen in the figure, the signal is negative at all times. The main part of the signal (about 80% of the signal at 540 nm) decreases at the system response. The smaller amplitude (of about 20% of the signal) increases with a time constant of about ∼1 ps.

Figure 6 shows the pump−probe spectra of HPTS in a neutral water solution in the wavelength region 500−620 nm at selected times. As seen, the spectrum changes its intensity as the time progresses. The spectra also narrow somewhat with time. Thus,

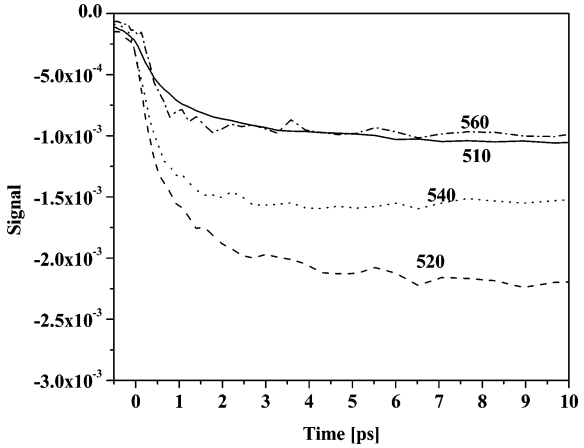

Figure 5. Pump−probe signal of HPTS in water at pH ∼ 10, probed at selected wavelengths.

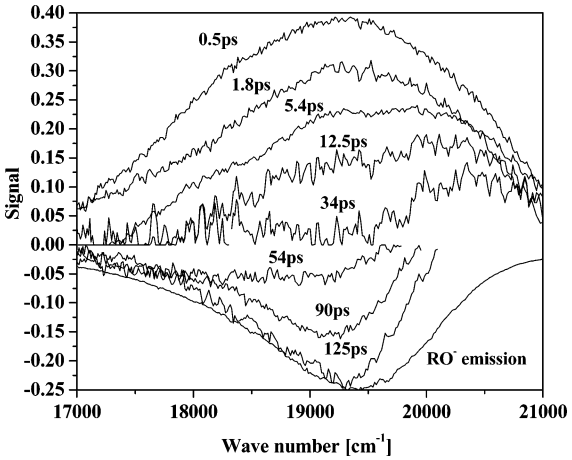

Figure 6. Pump−probe spectra of HPTS in a neutral water solution over the wavelength region 480−600 nm at selected times.

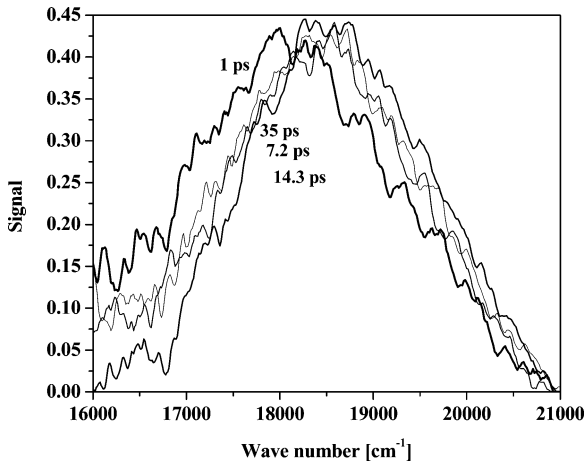

Figure 7. Pump−probe spectra, at selected times, of HPTS in a methanol solution.

the red part disappears faster and the blue part of the spectrum decays slower. At about 60 ps, the pump−probe signal turns negative.

Figure 7 shows the pump−probe spectra, at selected times, of HPTS in a methanol solution. In this solution, only the protonated ROH form exists in both the ground and excited states. In methanol solution, HPTS is incapable of transferring a proton within the excited-state lifetime and thus the shape of the pump−probe spectra shown in Figure 7 mostly resemble

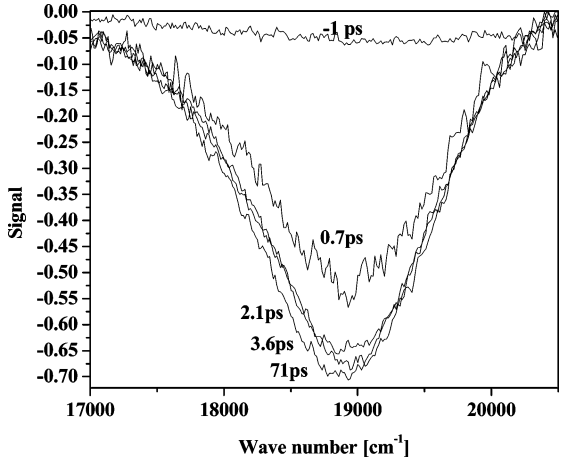

Figure 8. Pump−probe spectra of basic solution of HPTS (pH ∼ 10) at selected times.

the lowest excited-state absorption to higher excited states. As seen in Figure 7, the spectrum is positive at all times monitored (up to ∼100 ps) and the amplitude and shapes are almost constant at all times.

Figure 8 shows the pump−probe spectra of a basic solution of HPTS (pH ∼ 10) at selected times. As seen, the spectrum is negative at all times. The shape and amplitude of the spectra change only slightly with time. The spectrum narrows somewhat and shifts to the blue as time progresses. The negative signal of the basic solution arises from the strong stimulated emission signal of the RO^{-}* centered at about 520 nm.

Discussion

New Model for ESPT. In this paper, we wish to extend our previous diffusion-assisted excited-state proton-transfer model to include an additional reactive step (see Schemes 1 and 2). The excited protonated acid ROH* dissociates first to a contact ion pair, consisting of an anion and a hydrogen bonded hydrated proton complex, which we designate H_3O^+.

Agmon[39] suggested a particular structure for the contact ion pair formed after photoacid dissociation. The proton in the contact ion pair does not exist in the H_3O^+ or the $H_9O_4^+$ structures but rather in a symmetric dimmeric structure of $H_5O_2^+$ suggested by Zundel[40] and seen in X-ray structures of concentrated HCl.[41] The contact ion pair forms a pentameric ring structure consisting of the oxygen of the RO^- hydrogen bonded to a pair of water molecules and the ring is closed by two other water molecules forming the proton dimmer.

The contact ion pair RO^{-}*···H_3O^+ exhibits about the same spectroscopic signature as the RO^- emission band of the separated and solvated ion pair. The fluorescence band is broad and asymmetric and has a peak at about 512 nm. An important finding of the model fitting to the experimental data imposes that the equilibrium constant of the first step in the dissociation process is about 0.5. Thus, the time-dependent concentration of the contact ion pair is small at all times. The decrease of the ROH concentration in the first few picoseconds is rather small, only 30%. This decrease in excited ROH concentration is easily measured by femtosecond techniques such as fluorescence up-conversion or pump−probe; see Figure 3 of this paper and also data shown in Figure 4 of ref 11. In the TCSPC signal of the ROH fluorescence measured at 435 nm, the first dissociation step should decrease the ROH signal. But due to limited time resolution this decrease cannot be detected. In the rise time of the RO^- TCSPC signal measured at $\lambda > 520$ nm, a short-rise-

time component of about 22% is followed by a long 100 ps rise time (see Figure 1). It appears as an immediate rise time within the instrument response function of the TCSPC system. We interpreted this short-rise-time component over many years as arising from a large overlap between the emission of ROH and RO^- and also due to a direct excitation of the ground-state population of the conjugated base RO^-(g). The RO^-(g) concentration depends strongly on the solution pH. The pK_a of HPTS in water is about 7.7.[3] Figure 2 shows that the overlap between ROH and RO^- in neat ethanol solution at 520 nm is rather small and is about 8% or less.

We claim in this paper that the short component of about 3 ps in the pump−probe signals shown in Figure 3a,b and the inconsistency in the decay of ROH and rise in the RO^- TCSPC signals arise from the contribution of a missing step in the previous model of the proton-transfer reaction and the limited time resolution of the TCSPC technique. The product of the first step is probably a contact ion pair where the spectroscopic properties of the visible absorption and emission of the $RO^-{}^*\cdots H_3O^+$ are quite similar to that of a fully separated ion pair $RO^-{}^*- - -H_3O^+$. We used a simple kinetic model[42] to display the main features of the ESPT process:

$$A \underset{k'_r}{\overset{k'_{PT}}{\rightleftharpoons}} B \underset{k_r}{\overset{k_{PT}}{\rightleftharpoons}} C$$

$$[A]_t = [A]_0\left[\frac{k'_r k_r}{\gamma_1\gamma_2} + \left(\frac{{\gamma_1}^2 - \gamma_1(k'_r + k_{PT} + k_r) + k'_r k_r}{\gamma_1(\gamma_1 - \gamma_2)}\right)e^{-\gamma_1 t} + \left(\frac{{\gamma_2}^2 - \gamma_2(k'_r + k_{PT} + k_r) + k'_r k_r}{\gamma_2(\gamma_2 - \gamma_1)}\right)e^{-\gamma_2 t}\right] \quad (3a)$$

$$[B]_t = k'_{PT}[A]_0\left[\frac{k_r}{\gamma_1\gamma_2} + \left(\frac{k_{PT} - \gamma_1}{\gamma_1(\gamma_1 - \gamma_2)}\right)e^{-\gamma_1 t} + \left(\frac{k_r - \gamma_2}{\gamma_2(\gamma_2 - \gamma_1)}\right)\right]e^{-\gamma_2 t} \quad (3b)$$

$$[C]_t = k'_{PT}k_{PT}[A]_0\left[\frac{1}{\gamma_1\gamma_2} + \left(\frac{1}{\gamma_1(\gamma_1 - \gamma_2)}\right)e^{-\gamma_1 t} + \left(\frac{1}{\gamma_2(\gamma_2 - \gamma_1)}\right)e^{-\gamma_2 t}\right] \quad (3c)$$

where

$$\gamma_1 = -\frac{(-(k'_{PT} + k_{PT} + k'_r + k_r) + \Delta}{2} \quad (4a)$$

$$\gamma_2 = -\frac{(-(k'_{PT} + k_{PT} + k'_r + k_r) - \Delta}{2} \quad (4b)$$

and

$$\Delta = \sqrt{(k'_{PT} + k_{PT} + k'_r + k_r)^2 - 4(k'_{PT} + k_{PT} + k'_r k_r + k'_{PT} k_r)}$$

In our case, the fluorescence band shape and position of the intermediate product B ($RO^-{}^*\cdots H_3O^+$) and the C species ($RO^-{}^*- - -H_3O^+$) are about the same and, thus, the measured fluorescence is from either the excited photoacid ROH* with a peak at 440 nm or the combined *B*+*C* fluorescence at 512 nm arising from RO^-. The ABC model does not include the last step, the diffusion geminate-recombination of the proton and the conjugated base.

The first dissociation step is given by

$$H_2O + ROH \underset{k'_{rr}}{\overset{k'_{PT}}{\rightleftharpoons}} RO^-\cdots H_3O^+$$

The forward and the backward reaction rate constants, k'_{PT} and k'_r, are relatively fast $k'_{PT} \approx 0.6 \times 10^{11}$ s^{-1}, $k'_r \approx 2.2 \times 10^{11}$ s^{-1}, ($\tau'_{PT} \approx 14$ ps). In our model, we use a pseudo-first-order rate constant for the recombination rate constant k'_r. The 3 ps component observed in the ultrafast experiments is somewhat misleading for deducing the actual rate of the dissociation k'_{PT} of the acid. It arises from the faster recombination rate constant k'_r. The overall observed fast rate is given by the constant γ_1 in the ABC model (see eq 4a). It is a sum of the forward and backward rate constants. The second reactive step involves the separation of the proton from the anion by at least a single water molecule to form a separated and solvated ion pair. The second step involves much slower forward and backward rates

$$RO^-\cdots H_3O^+ \underset{k_r}{\overset{k_{PT}}{\rightleftharpoons}} RO^- - - -H_3O^+$$

$k_{PT} = 3.5 \times 10^{10}$ s^{-1} ($\tau_{PT} \approx 28.6$ ps) and k_r, the intrinsic geminate recombination rate constant $k_r = \kappa_a/4\pi a^2 \approx 5 \times 10^{10}$ M^{-1} s^{-1}; $\kappa_a \cong 0.008$ ps/Å.[16] The second reactive step, followed by the diffusion-assisted geminate recombination of the proton with the excited conjugated base RO^-*, is quantitatively described by our previous model.[16,22]

Because the first-step rate constants are larger than the second-step rate constants, k'_{PT}, $k'_r \gg k_{PT}$, k_r, the decrease of the population of ROH* is biphasic, the first step involves the reduction of the ROH* population by about ∼30% to form a contact ion pair. The contact-ion-pair concentration is limited because the equilibrium constant, K'_{eq}, is about 0.5 and the second step involves much slower processes.

Time-Resolved Single Wavelength Measurements. *Short Time.* Figure 9 shows the plot of the ABC model calculation of $[A]_t$, the protonated form ($[B]_t + [C]_t$), the combined contribution of $RO^-{}^*\cdots H_3O^+$ and $RO^-{}^*- - -H_3O^+$, and the separate contributions of $[B]_t$ and $[C]_t$ as a function of time with rate constants given in Table 2. The rate constants chosen for the plots of Figure 9 are those that best fit the pump−probe signal as well as the TCSPC signals of both ROH and RO^- fluorescence. We clearly see in Figure 9 the nature of the two-reactive-step model. The ROH band decays in two phases—a short one of about 3 ps with an amplitude of about 0.3 and a long-time component of about 100 ps with amplitude of 0.7. The RO^-* signal increases in two phases—one of about 3 ps and the second one in 100 ps.

The pump−probe signal of HPTS in neutral water is approximated by a superposition of the absorption of the ROH and RO^-, from the first excited state to higher excited states and the stimulated emission of the ROH form and the RO^- form. In the spectral range $\lambda > 500$ nm, the contribution of the emission of the ROH is small and the absorption of RO^-* to a higher excited state is also small (see Figure 8). The pump−probe measured signal at a specific wavelength λ in the long wavelength 520−600 nm range can be approximated by

$$PPS_\lambda(t) \propto a_1\sigma(\lambda)^{ROH}_{S_1\rightarrow S_2}c_t^{ROH} - b_1\sigma(\lambda)^{RO^-}_{S_1\rightarrow S_0}[c_t^{RO^-\cdots H^+} + c_t^{RO^- - - -H^+}] + c_1[\exp(-k_\Delta t)] \quad (5a)$$

TABLE 2: Kinetic Parameters for the Proton-Transfer Reaction of HPTS in Water Using the ABC Model (Scheme 2)

	k'_{PT} [10^{11} s^{-1}]	k'_r[a] [10^{11} s^{-1}]	k_{PT} [10^{10} s^{-1}]	k_r [10^9 M^{-1} s^{-1}]	τ_s[b] [ps]	τ_f[c] [ns]	γ_1[d] [s^{-1}]	γ_2 [s^{-1}]
HPTS/H_2O	0.60	2.20	3.5	1.5	0.8	5.4	3.01×10^{11}	7.3×10^9
HPTS/D_2O	0.3	1.30	2.0	1	0.8	5.4	1.7×10^{11}	4.5×10^9

[a] k'_r is a pseudo-first-order rate constant. [b] τ_s is the solvation time constant, $\tau_s = 1/k_\Delta$ (k_Δ appears in eq 5 and in eq 8). [c] τ_f is the excited-state lifetimes of both ROH and RO^-. [d] See eq 3 in the text.

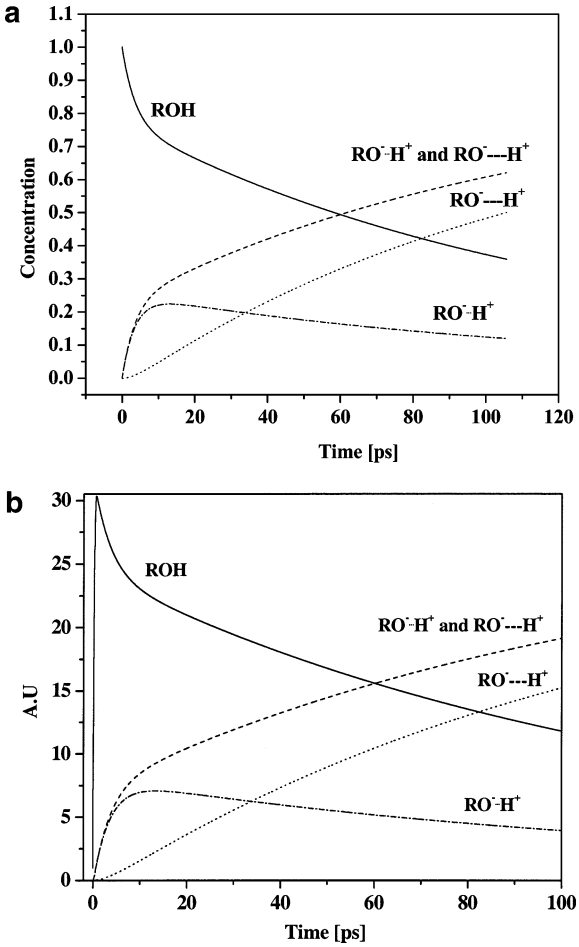

Figure 9. ABC model calculation: (a) $[A]_t$, ($[B]_t + [C]_t$), as well as $[B]_t$ and $[C]_t$ as a function of time (see text). (b) Convoluted with TCSPC IRF of 35 ps.

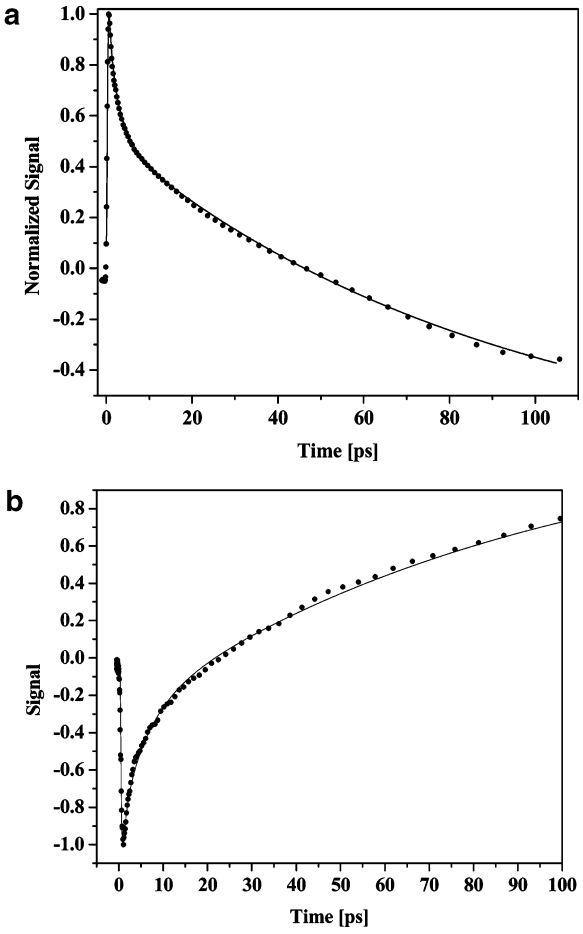

Figure 10. Fit of the pump−probe signals of HPTS in water by the ABC model and using eq 5: (a) measured at 540 nm; (b) measured at 430 nm.

the pump−probe signal measured at 430 nm the signal is given by

$$\mathrm{PPS}_\lambda(t) \propto a_2\sigma(\lambda)^{RO^-}_{S_1\rightarrow S_2}[c_t^{RO^{-}\cdots H+} + c_t^{RO^{-}---H+}] - b_2\sigma(\lambda)^{ROH}_{S_1\rightarrow S_2}c_t^{ROH} - c_2[\exp(-k_\Delta t)] \quad (5b)$$

for where *a*, *b*, and c are adjustable amplitudes, $\sigma(\lambda)^{ROH}_{S_1\rightarrow S_2}$ and $\sigma(\lambda)^{RO^-}_{S_1\rightarrow S_2}$ are the absorption cross sections for the excited-state absorption of ROH or RO^- to higher excited states. $\sigma(\lambda)^{ROH}_{S_1\rightarrow S_0}$ and $\sigma(\lambda)^{RO^-}_{S_1\rightarrow S_0}$ are the emission cross sections from $S_1 \rightarrow S_0$ for RO^- and ROH. c_t^{ROH}, $c_t^{RO^-\cdots H^+}$, and $c_t^{RO^{-}---H^+}$ are the time-dependent concentrations of the acid form, the contact ion pair, and the solvated ion pair, respectively. The term $c[\exp(-k_\Delta t)]$ probably arises from the solvation dynamics of the reactant and products or vibration energy redistribution and subsequent cooling of the ROH. These processes were also observed by previous studies.[10,11,47] These processes are also observed as changes in the pump−probe spectra as a function of time (see Figure 6) and discussed below.

Figure 10a shows the normalized pump−probe signal of HPTS in water measured at 540 nm along with a computer fit. Figure 10b shows the experimental results of the pump−probe signal at 430 nm shown in Figure 3b along with the fit (solid line) based on the A ⇄ B ⇄ C model and calculated using eq 5b. The computed signal (shown as a solid line in the figures) is convoluted with the pump−probe system response using a cross correlation of about 250 fs fwhm. As seen in Figure 10a,b, the fits are rather good. The fitting parameters of Figure 10a are $a_1 = 1$, $b_1 = 1.55$ and $c_1 = 0.31$ and for 10b are $a_2 = 1$, $b_2 = 1.65$ and $c_2 = 0.25$. The rate constants of the ABC model for the probe signals in the green and the blue regions are the same and are given in Table 2.

Long Time. Figure 11a shows, on an extended time scale the computed time-dependent concentrations of ROH, $[A]_t$, $RO^{-}*\cdots H_3O^+$, $[B]_t$ $RO^{-}*---H_3O^+$, $[C]_t$, and the combined RO^- concentrations $\{[B]_t + [C]_t\}$. The short-time decay and rise of $[A]_t$ and $\{[B]_t + [C]_t\}$, respectively, is clearly seen. The time-dependent combined concentrations $[B]_t + [C]_t$ provide the total RO^- concentration. It is monitored by following the time-resolved fluorescence measured by the TCSPC technique.

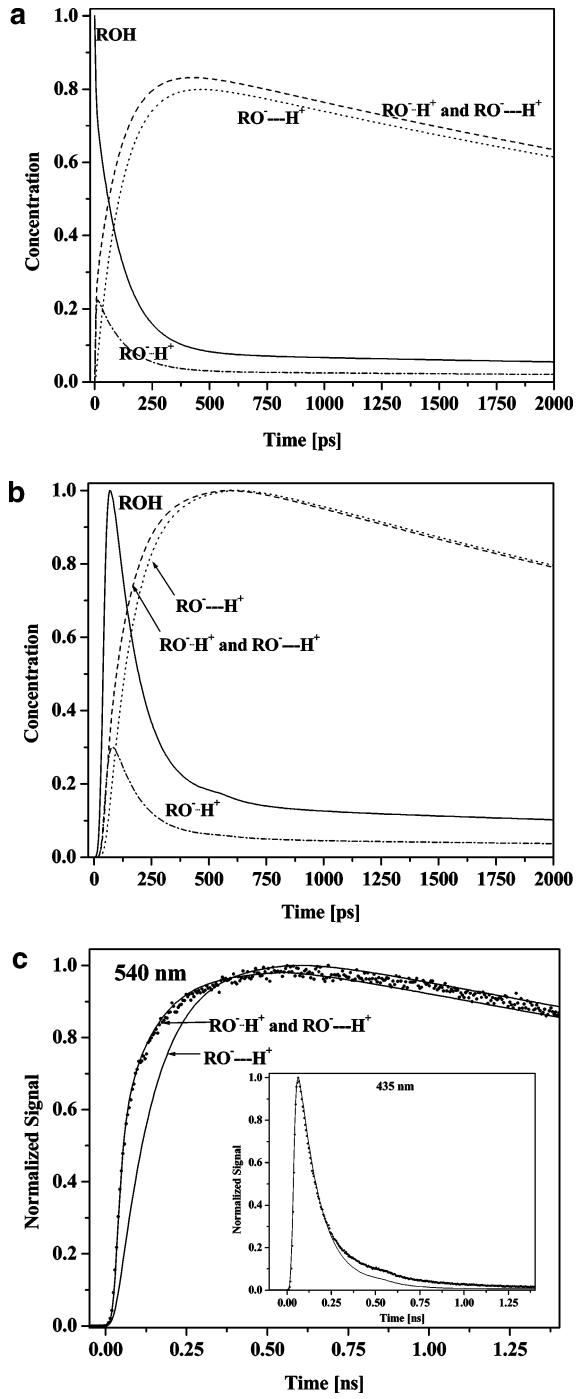

Figure 11. ABC model calculations. (a) Computed time-dependent concentrations of ROH, $[A]_t$, $RO^{-}{}^{*}\cdots H^{+}$, $[B]_t$, $RO^{-}{}^{*}- - -H^{+}$, $[C]_t$, and the combined RO^{-} concentrations $\{[B]_t + [C]_t\}$ (see text). (b) ABC model concentrations convoluted with the IRF of the TCSPC. (c) Plots of the same computer fits at longer times along with the experimental TCSPC signals of both ROH (measured at 435 nm) and RO^{-} (measured at 520 nm).

Figure 11b shows the ABC model concentrations convoluted with the IRF of 35 ps of the TCSPC system. The signal of the ROH fluorescence does not show the short-time small amplitude component of about 3 ps seen in Figure 11a. The rise-time of RO^{-} of the time-resolved fluorescence signal shows a fast component with an amplitude of about 0.2 and a long component of amplitude of 0.8 with a rise-time of about 100 ps. The fast component of the $RO^{-}{}^{*}$ rise-time cannot be resolved in time due to the 35 ps system response. The overall effect of the slow response of the TCSPC is that the short-time component is totally missing in the time-resolved ROH emission measurement whereas the RO^{-} signal has an immediate rise-time with an amplitude of about 0.2. Over many years of our research we overlooked the fine detail that leads to the inconsistency between the initial decay time of about 100 ps of the ROH and the biphasic rise RO^{-}.

Figure 11c shows the plots of the same computer fits of Figure 11b along with the experimental TCSPC signals of both the ROH measured at 435 nm and the RO^{-} at 520 nm. The computed signals are convoluted with the TCSPC system response of about 35 ps. Because the lifetimes of ROH and RO^{-} are similar, $\tau_f \approx 5.4$ ns, we multiplied the populations given in eq 3 by $\exp(-t/\tau_f)$. As seen in Figure 11c, the short-time component of the ROH decay is absent in the TCSPC signal as well as the convoluted computer fit. The rise time of the RO^{-} is biphasic with short and long-time components. The fit of the computed signal to the experimental ROH is only good for short times because the ABC cannot accurately reproduce the nonexponential decay arising from the diffusion-assisted geminate recombination step.

Two Kinetic Steps Followed by a Diffusion Step. A more realistic calculation than the ABC model of both the pump−probe signal and the long-time behavior, given accurately by TCSPC measurements, should also include the proton-transfer dynamics in the diffusion space. For this purpose we used a modified configuration of the SSDP program[34] (shown in Scheme 2) to calculate the ROH, $RO^{-}\cdots H_3O^{+}$, and RO^{-} populations.

In Scheme 2, the two reactive steps, are followed by a diffusion step.

The last step accurately describes the reversible geminate recombination process between the proton and the solvated excited conjugate photobase. In the ABC model, the diffusive part is described by exponential kinetics and hence the long-time ROH decay cannot be fitted to a satisfactory level; see Figure 11c. Figure 12a shows the diffusional model fit of the time-resolved emission of ROH measured at 435 nm, as measured by the TCSPC technique. As seen in the figure, the convoluted computer fit is very good at all times. Figure 12b shows the computed signal prior to convolution with a rather broad TCSPC instrument response function of 35 ps. The short-time component of about 3 ps lifetime and amplitude of 25% of the signal is clearly seen. The parameters of the fitting are given in Table 3. There are four kinetic parameters, k'_{PT} and k_{PT}, the forward proton-transfer rate constants and the backward, recombination rate constants: k'_r and k_r. The short-time component of about 3 ps is mainly determined by the sum of the rate constant of the first kinetic stage $k = k'_{PT} + k'_r$. The amplitude of the short-time component is roughly given by $k'_{PT}/(k'_{PT} + k'_r)$. Because $k'_r \sim 3k'_{PT}$, the amplitude of the short time is small—about 25% of the signal. The second time component decays at about 100 ps.

Using the proposed three-step extended model, the relatively long 100 ps time component arises from two main contributions that act stepwise in time. The value of both forward proton-transfer rate constants, k'_{PT} and k_{PT}, mainly determines the 100 ps time component. These rate constants, $k'_{PT} = 60$ ns^{-1} ($\tau'_{PT} \sim 15$ ps) and $k_{PT} = 40$ ns^{-1} ($\tau_{PT} \sim 25$ ps), are almost equal. Though each individual time constant is rather short, the overall complex multistage model second decay is relatively long (100 ps). The last and longest time component of the ROH transient population is nonexponential and arises from the reversible geminate recombination of the diffused proton, at the contact radius of the RO^{-} solvated form of HPTS, which is placed at

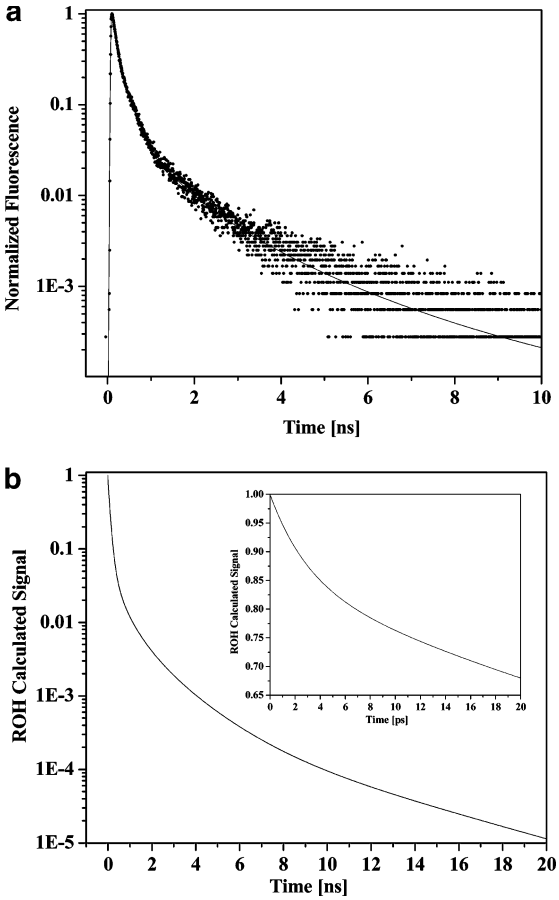

Figure 12. Time-resolved emission of HPTS ROH form in H_2O measured at 435 nm (dot) and computer fit using the extended geminate recombination model; see text (solid line). The computed signal is convoluted with the IRF of the TCSPC system.Computed signal only.

TABLE 3: Kinetic Parameters for the Proton-Transfer Reaction of HPTS Water Using the Modified Geminate Recombination Model (SSDP Fit), $R_D = 28$Å

	k'_{PT} [ns^{-1}]	k'_r[a] [ns^{-1}]	k_{PT} [ns^{-1}]	k_r [Å ns^{-1}]	D [cm^2 s^{-1}]	τ_{ROH}- [ns]	τ_{RO^-}- [ns]
HPTS/H_2O	60	220	50	6.5	1.0×10^{-4}	5.4	5.4
HPTS/D_2O	15	60	22	6.0	7.5×10^{-5}	5.4	5.4

[a] k'_r is a pseudo-first-order rate constant.

about $a \sim 6$ Å. The radius of the bare HPTS is only 3 Å. If one includes one solvation shell surrounding HPTS, the radius increases to about 5.5 Å. This value is also deduced from the measured time-resolved fluorescence anisotropy and the fit to a rotating sphere with stick boundary condition.

Isotope Effect. Figure 13 shows the pump probe experimental signal of HPTS in both H_2O and D_2O. The probe wavelength is set to 540 nm. As seen, the D_2O signal consists of short and long-time components that are similar but slower than those in H_2O. Solvation dynamics experiments revealed that the solvation dynamics[43,44] of coumarin dyes in both H_2O and D_2O are very similar. The solvation dynamics of water is bimodal and consists of two components: an ultra short component of <50 fs and a longer component of about 0.8 ps.

Thus, we attribute the large difference in the pump−probe signal to the slower rates of proton transfer in both stages: the first one forms a contact pair, and in the subsequent step, the separated ion pair is formed.

The pump−probe signal of HPTS in D_2O, as seen in Figure 13, has a short component of about 5 ps with a small amplitude

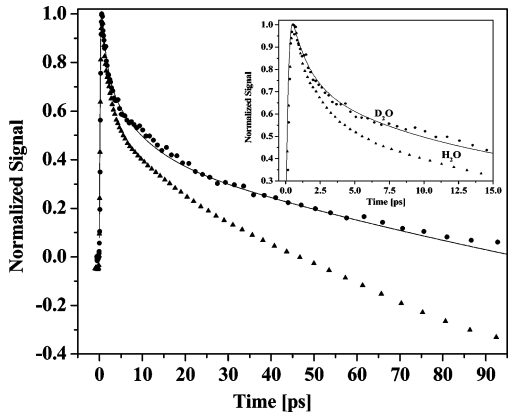

Figure 13. Pump−probe signal of HPTS in D_2O solution along with a computer fit using ABC model. The probe signal is measured at 540 nm. For comparison, the results of water samples are also shown

of about 30% followed by a long component of about 250 ps. In time-resolved emission measurements (not shown) measured by the TCSPC technique with 35 ps IRF, we sample only the long component of about 300 ps in D_2O. Thus, the isotope effect is a factor of 3 for the long component. We used the ABC model and eq 5 to fit the pump−probe signal of HPTS in D_2O excited at about 400 nm and probed at 540 nm. The fitting parameters are given in Table 2. The three rate constants, k'_{PT}, k_{PT} and k'_r, are smaller by about a factor of 2 than the values we find for water.

Pump−Probe Spectra. The pump−probe spectra of HPTS in various solutions, excited by a pump pulse at ∼395 nm and probed by a supercontinuum at long wavelengths $\lambda > 490$ nm, are shown in Figures 6−8. Figure 6 shows the pump−probe transient spectra of HPTS in a neutral water solution in the wavelength region 500−620 nm at selected times. As seen, the transient spectrum at $t \sim 0.5$ ps is positive. The intensity reduces to zero over time and, in the wavelength region 510−580 nm, the transient spectra changes sign to a negative signal at about 50 ps. As the time further progresses, the spectra also shift to the blue and narrow somewhat. Thus, the red part disappears faster and the blue part of the spectrum decays slower.

In a methanol solution, HPTS is incapable of transferring a proton within the excited-state lifetime. In this solution, only the protonated ROH form exists in both the ground and excited states. The shape and position of the pump−probe transient spectra shown in Figure 7 mainly resemble the lowest excited-state absorption. As seen in Figure 7, the spectra are positive for all times monitored (up to ∼100 ps) and the amplitude and shapes are almost constant.

Figure 8 shows the pump−probe transient spectra of a basic solution of HPTS (pH ∼ 10) at selected times. As seen, the spectra are negative at all times. The shape and the amplitude of the spectra change only slightly with time. The spectra narrow somewhat as time progresses. The negative signal of the basic solution arises from the strongly stimulated emission signal of the RO^-* centered at about 520 nm.

The fit of the pump−probe spectra of Figure 6 is based on the new model presented above and is given schematically in Scheme 2. The pump−probe spectra of Figure 6 were fitted according to

$$\mathrm{PPS}(\omega,t) \propto f^{\mathrm{ROH}}(\omega,t)c_t^{\mathrm{ROH}} - g^{\mathrm{RO^-}}(\omega,t)[c_t^{\mathrm{ROH^-\cdots H^+}} + c_t^{\mathrm{RO^- - - -H^+}}] \quad (6)$$

where $f^{\mathrm{ROH}}(\omega,t)$ and $g^{\mathrm{RO^-}}(\omega,t)$ are the line shape functions of

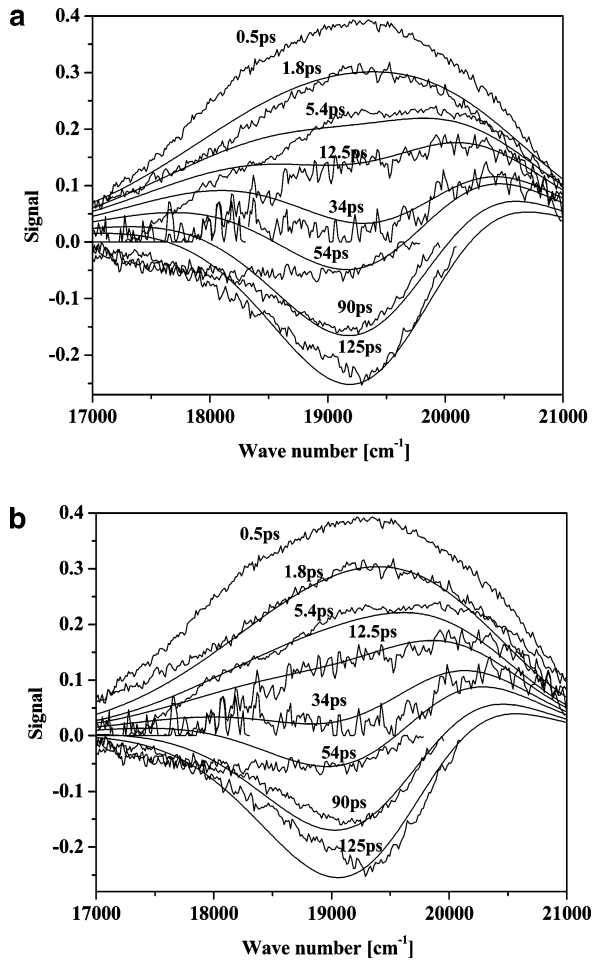

Figure 14. Fit of the HPTS pump−probe spectra at selected times using the ABC model. Note that the kinetic fitting parameters are the same as those used for Figures 10a and 11b (given in Table 2). (a) The ROH line-shape function, $f^{ROH}(\omega,t)$ is time-independent. (b) The ROH spectrum bandwidth decreases by about 500 cm^{-1} with a time constant of 800 fs.

the ROH absorption and the RO^- stimulated emission, respectively. c_t^{ROH}, $c_t^{RO^-\cdots H^+}$, $c_t^{RO^-\ -\ -\ -H^+}$ are the time-dependent concentrations of the acid form, the contact ion pair, and the solvated ion pair, respectively. The time-dependent concentrations of the various species are calculated by the ABC model using eqs 3a−c.

Figure 14a shows such a fit to the pump−probe spectra at selected times. The stimulated emission line shape spectrum, $g^{RO^-}(\omega,t)$, was taken from the RO^- pH ∼ 10 pump−probe spectra shown in Figure 8. The line shape spectra for ROH, $f^{ROH}(\omega,t)$, is the same as the spectrum of HPTS in water at 5.5 < pH < 6.5 at time 0.5 ps (Figures 6 and 14). Each of the normalized line shape functions, $f(\omega,t)$ and $g(\omega,t)$, we first fit to a log-normal function with adjustable parameters Δ, ν_p, h, and γ. The shape of the absorption and fluorescence bands of dye molecules in polar solvents is well described by a log-normal function,[45]

$$I(\nu) = h\begin{cases}\exp[-\ln(2)\{\ln(1+\alpha)/\gamma\}^2] & \alpha > -1\\ 0 & \alpha \le -1\end{cases} \qquad (7)$$

where $\alpha \equiv 2\gamma(\nu - \nu_p)/\Delta$, $I(\upsilon)$ is the fluorescence intensity at frequency (υ), h is the peak height, ν_p is the peak frequency, γ is the asymmetry parameter, and Δ represents the bandwidth. This four-parameter function describes an asymmetric line shape which reduces to a Gaussian one in the limit $\gamma = 0$.

TABLE 4: Log-Normal Parameters of Both the ROH and RO^- Pump−Probe Spectra

	ν_p [cm^{-1}]	Δ_0[cm^{-1}]	h	γ	ΔΔ [cm^{-1}][a]
ROH	19 300	2800	0.39	−0.1	500
RO^-	19 100	1600	0.665	−0.17	0

[a] See eq 7.

The fit is rather good on the high-energy side and quite poor on the low-energy side. As seen in Figure 14a, the pump−probe spectra at the low frequencies decay to zero for short times and the overall effect is a smaller bandwidth. This phenomenon can be explained as arising from (1) solvation dynamics, (2) hydrogen bond dynamics, and (3) excess vibration energy of the excited state at $t = 0$ leading to the increase of spectral bandwidth. This is followed by a vibration energy dissipation to the solvent and subsequent cooling of the solvent molecules surrounding the excited ROH* molecule.

Pines et al. studied the excited-state hydrogen bond dynamics of an HPTS analogue, 8-hydroxy-1,3,6-tris(dimethylsulfonamide) (HPTA), in mixtures of DCM−DMSO.[46] The DMSO is strongly complexed to HPTA with an equilibrium constant of $K_{eq} = 358\ M^{-1}$ and, thus, even a small amount of DMSO (∼10^{-2} M) in the mixture is enough to cause a large fraction of complexed HPTA−DMSO in solution. They found that the hydrogen bonding dynamics due to excitation by a 400 nm pulse is short on the order of 55 ± 10 fs.

The width of the pump−probe band shape of the ROH signal, Δ, shrinks at short times. The time-dependent narrowing of the width is accounted for by the following expression

$$\Delta = \Delta_0 - \Delta\Delta(1 - \exp(-k_\Delta t)) \qquad (8)$$

where Δ_0 is the bandwidth in wavenumber at $t = 0$, ΔΔ ∼ 500 cm^{-1} is the decrease of the bandwidth for long times, and k_Δ is the rate constant of the bandwidth decrease.

Figure 14b shows the model fit using eq 6 and includes the time-dependent bandwidth narrowing (eq 8). As seen, the fit is rather good at all times. For the time-dependent bandwidth narrowing, we used $k_\Delta \sim 1.2 \times 10^{12}\ s^{-1}$. This rate constant is also used to fit the fastest decay component of the time-resolved pump−probe signal measured at 540 nm shown in Figure 10a. The log-normal parameters of both the ROH and RO^- pump−probe spectra are given in Table 4.

Comparison with the Results and Models of Other Groups. Prayer et al.[10] used femtosecond fluorescence up-conversion and Tran-Thi et al.[11] used pump−probe spectroscopies to probe the early events of the excited-state proton transfer (ESPT) from HPTS to water. Both studies found that the process involves two ultrafast steps (300 fs and 2.5 ps) that precede the relatively slow (87 ps) proton-transfer step. These ultrafast steps were identified by the authors as the solvation dynamics of the locally excited (LE) state of the acid and its subsequent relaxation to an intermediate CT electronic state. Prayer et al.[10] found that in aqueous solutions of pH = 4, the excited HPTS ROH* fluorescence shifts in time to the red, and its integrated intensity decreases by about 50% (shown in Figure 3 of ref 10) with a time constant of about 2.2 ps.[10] The fluorescence signal of the RO^-*, measured at 515 nm, increases with two time components—an ultrashort one and a 87 ps long one (Figure 4 of ref 10). The amplitude of the fast component is about ∼30%. The time dependence of the RO^- up-conversion[10] signal and this study TCSPC measurement are similar. The signal rise time of both measurements consists of short- and long-time components with similar relative amplitudes. Prayer et al.[10] proposed a mechanism

similar to the model we proposed in this paper. In their photoacid dissociation scheme, the formation of a contact ion pair takes place within 2.2 ps. The ion pair dissociates into free ions with a time constant of 87 ps. In a later paper by Tran-Thi et al.[11] the short, 3 ps, component was attributed to the relaxation of the initially prepared excited LE state to the CT state.

In contrast to their latest model,[11] in our model the short component of 3 ps of the pump−probe signal is not attributed to the formation of a CT state but to the formation of a contact ion pair. This process is much faster than the preceding step, of about 100 ps, to form a separated noncontact ion pair.

The two-reactive-step model has similarities with the model of Ando and Hynes on the dissociation mechanism of HCl and other acids.[28] They found that the mechanism involves two reactive steps. The first is a nearly activationless motion in a solvent coordinate, which is adiabatically followed by the quantum proton rather than tunneling, to produce a contact ion pair $Cl^--H_3O^+$, which is stabilized by ~7 kcal/mol. The second step includes the motion in the solvent with a small activation barrier, as a second adiabatic proton transfer produces a solvent-separated ion pair from the contact ion pair in a nearly thermoneutral process. Motion of a neighboring water molecule, to accommodate the change of the primary coordination number from 4 for H_2O to 3 for H_3O^+ of a proton-accepting water molecule, is indicated as a key feature in the necessary solvent reorganizations.

The two reactive steps in our qualitatively revised model are similar to the model proposed by Prayer et al.,[10] and also to the quantitative model of Ando and Hynes for dissociation of a strong acid such as HCl. The chemical kinetic ABC model describes only schematically the complex ESPT process. The fitting parameters of our model are the forward and backward rate constants of the two reactive steps. The experimental results of HPTS studies impose an additional constraint. The amplitude of the decrease in the concentration of the acid form due to the first fast step is limited to only a small fraction of about 0.3. To achieve such a small dissociation fraction, we impose that the back-reaction rate constant k'_r (see Scheme 2), should be larger than k'_{PT} by about a factor of 2. The 3 ps component observed in the ultrafast experiments is somewhat misleading for deducing the actual rate of the dissociation k'_{PT} of the acid. It arises from the faster recombination rate constant k'_r. The overall observed fast rate constant γ_1 in the ABC model (eq 4) is given as a sum of the forward and backward rate constants. The experimental observations indicate that the larger fraction of the ROH concentration decays at about 100 ps.

Conclusions

Our recent experiments, using ultrafast techniques,[47,48] as well as those by Prayer et al.[10] and Tran-Thi and co-workers,[11] showed that short-time components exist in both the fluorescence up-conversion and the pump−probe signal of an HPTS water solution. The theoretical work by Hynes and co-workers[28] shows also that the acid dissociation process can be divided into two steps. In past experiments on ESPT, we used the TCSPC technique with an instrument response function of only about 35 ps fwhm. The initial decay time of the ROH fluorescence measured by the TCSPC technique at 435 nm is 100 ps whereas the rise time of the RO^- exhibits two time components, one of a very short time, <20 ps, and the other having a long time, 100 ps. In the past, we explained the inconsistency between the ROH decay time and the biphasic rise time of the RO^- by several reasons but never looked at it more cautiously. In this paper, we claim that the inconsistency in the TCSPC time-resolved emission signal of the decay of the ROH and complementary rise of RO^- arises from a missing step in the mechanism of the proton-transfer reaction. The product of the first step of the photoacid dissociation is a contact ion pair $RO^-*\cdots H_3O^+$ where the spectroscopic properties of the visible absorption and emission are quite similar to those of a fully solvated and separated ion pair, $RO^-*- - -H_3O^+$; i.e., the emission spectroscopy of the RO^- form is only slightly sensitive to the proton position.

On the basis of pump−probe measurements of both ROH and RO^- signals, we developed a new model for intermolecular ESPT to a solvent. The model includes two reactive steps followed by a diffusion-assisted step. The model accounts for the following experimental observations.

1. The time dependence of the excited photoacid ROH* concentration is biphasic with decay times of ~3 and 100 ps and relative amplitudes of about 0.3 and 0.7, respectively (the pump−probe signal is shown in Figure 3b).

2. The time dependence of the formation of the excited deprotonated form, RO^-, is also biphasic with about the same characteristic times and amplitudes as for the ROH decay (the pump−probe signal is shown in Figure 3a).

3. A two-reactive-step mechanism, followed by a diffusion step, fits the experimental data well. The acid first dissociates to form a contact ion pair $RO^-*\cdots H^+$ at about 10 ps. The equilibrium constant of the first step is about 0.5. Thus the protonated form, ROH*, concentration decays to a value of about 0.7.

4. The 3 ps component observed in the ultrafast experiments is somewhat misleading for deducing the actual rate of the dissociation k'_{PT} of the acid. The 3 ps component arises from the faster recombination rate constant k'_r. The overall observed fast rate constant, determined by γ_1 in the ABC model is given as a sum of the forward and backward rate constants.

5. In the second reactive step, the contact ion pair separates by further solvation of both the RO^- and the proton. The rate of this step is slow, $\tau_{PT} = 28$ ps.

6. The third step involves the diffusion-assisted reversible geminate recombination of the proton with the excited conjugated base.

7. In TCSPC measurements of the time-resolved fluorescence of the ROH, the first fast step that leads to a partial decay of the ROH concentration is not observed at all. It appears at the RO^- luminescence as a fast rise time component with amplitude of about 0.22, much larger than the fluorescence overlap of the ROH and RO^- at the measured wavelength of 520 nm (about 11%).

Acknowledgment. We thank Professor N. Agmon, Professor E. Pines, and Dr. D. Pines for their valuable comments. This work was supported by grants from the Binational U.S.-Israel Science Foundation, and the James-Franck German-Israel Program in Laser-Matter Interaction.

Supporting Information Available: A detailed procedure to estimate the overlap between ROH and RO^- emission in water solution at 520 nm. This material is available free of charge via the Internet at http://pubs.acs.org.

References and Notes

(1) Bell, R. P. *The Proton in Chemistry*, 2nd ed.; Chapman and Hall: London, 1973.

(2) *Proton-Transfer Reaction*; Caldin, E. F., Gold, V., Eds.; Chapman and Hall: London, 1975.

(3) (a) Weller, A. *Prog. React. Kinet.* **1961**, *1*, 189, (b) *Z. Phys. Chem. N. F.* **1958**, *17*, 224.
(4) (a) Eigen, M. *Angew. Chem., Int. Ed.* **1964**, *3*, 1. (b) Eigen M.; Kruse W.; Maass G.; De Maeyer, L. *Prog. React. Kinet* **1964**, *2*, 285.
(5) Ireland, J. E.; Wyatt, P. A. *Adv. Phys. Org. Chem.* **1976**, *12*, 131.
(6) (a) Gutman, M.; Nachliel, E. *Biochim. Biophys. Acta* **1990**, *391*, 1015. (b) Pines, E.; Huppert, D. *J. Phys. Chem.* **1983**, *87*, 4471.
(7) Kosower, E. M.; Huppert, D. *Annu. Rev. Phys. Chem.* **1986**, *37*, 127.
(8) Tolbert, L. M.; Solntsev, K. M. *Acc. Chem. Res.* **2002**, *35*, 1.
(9) Rini, M.; Magnes, B. Z.; Pines, E.; Nibbering, T. J. *Science* **2003**, *301*, 349.
(10) Prayer, C.; Gustavsson, T.; Tarn-Thi, T. H. In *Fast Elementary Processes in Chemical and Biological Systems*; 54th International Meeting of Physical Chemistry; AIP: New York, 1996; pp 333.
(11) Tran-Thi, T. H.; Gustavsson T.; Prayer, C.; Pommeret S.; Hynes J. T. *Chem. Phys. Lett*. **2000**, *329*, 421.
(12) Smith, K. K.; Huppert, D.; Gutman, M.; Kaufmann, K. *J. Chem. Phys. Lett*. **1979**, *64*, 22.
(13) Clark, J. H.; Shapiro, S. L.; Campillo, A. J.; Winn, K. J. *J. Am Chem. Soc*. **1979**, *101*, 746.
(14) Politi, M. J.; Fendler, J. H. *J. Am. Chem. Soc.* **1984**, *106*, 265.
(15) Pines, E.; Huppert, D. *Chem. Phys. Lett.* **1985**, *116*, 295.
(16) Agmon, N.; Pines, E.; Huppert, D. *J. Chem. Phys.* **1988**, *88*, 5631.
(17) Pines, E.; Huppert, D. *J. Am. Chem. Soc.* **1989**, *111*, 4096.
(18) Pines, E.; Huppert, D.; Agmon, N. *J. Chem. Phys.* **1991**, *85*, 666.
(19) Agmon, N.; Huppert, D.; Masad, A.; Pines, E. *J. Phys. Chem.* **1991**, *96*, 952.
(20) Huppert, D.; Goldberg, S. Y.; Masad, A.; Agmon, N. *Phys. Rev. Lett.* **1992**, *68*, 3932.
(21) Agmon, N. *J. Phys. Chem. A* **2005**, *109*, 13.
(22) Agmon, N.; Pines, E.; Huppert, D. *J. Chem. Phys.* **1988**, *88*, 5631.
(23) Smoluchowski, M. von. *Ann. Phys*. **1915**, *48*, 1103.
(24) Debye. P. *Trans. Electrochem. Soc.* **1942**, *82*, 265.
(25) Kolodney, E.; Huppert, D. *Chem. Phys*. **1981**, *63*, 401.
(26) Pines, E., Huppert D., *J. Chem. Phys*. **1986**, *84*, 3576.
(27) Pines, E.; Huppert, D.; Agmon, N. *J. Chem. Phys.* **1988**, *88*, 5620.
(28) (a) Ando, K.; Hynes, J. T. In *Structure, Energetics and Reactivity In Aaqueous Solution*; Cramer, C. J., Truhlar, D. G., Eds.; American Chemical Society: Washington, DC, 1994. (b) Ando, K.; Hynes, J. T. *J. Phys. Chem. B* **1997**, *101*, 10464.
(29) Rini, M.; Pines, D.; Magnes, B.-Z.; Pines, E.; Nibbering, E. T. J. *J. Chem Phys*. **2004**, *121*, 9593.
(30) Debye, P. *Trans. Electrochem. Soc.* **1942**, *82*, 265.
(31) Poles, E.; Cohen, B.; Huppert, D. *Isr. J. Chem.* **1999**, *39*, 347.
(32) Förster, Th.; Volker, S. *Chem. Phys. Lett.* **1975**, *34*, 1.
(33) Förster, Th. *Pure Appl. Chem.* **1970**, *24*, 443.
(34) Krissinel, E. B.; Agmon, N. *J. Comput. Chem*. **1996**, *17*, 1085.
(35) Agmon, N.; Goldberg, S. Y.; Huppert, D. *J. Mol. Liq.* **1995**, *64*, 161.
(36) Robinson, R. A.; Stokes R. H. *Electrolyte Solutions*, 2nd ed; Butterworth: London, 1959; Appendices 1.1 and 6.2.
(37) Lewis, G. N.; Doody, T. C. *J. Am. Chem. Soc*. **1933**, *55*, 3504.
(38) Haar, H. P.; Klein U. K. A.;. Hfiner, F. W.; Hauster M. *Chem. Phys. Lett*. **1977**, *49*, 416.
(39) Agmon, N. *J. Mol. Liq*. **2000**, *85*, 87.
(40) Zundel, G. In *The Hydrogen Bond Recent Developments in Theory and Experiments*; Schusten, P., Zundel, G., Sandorfy, C., Eds.; North-Holland, Amsterdam, 1976; pp 687−766.
(41) Trio R.; Narten, A. H. *J. Chem. Phys*. **1975**, *63*, 3624.
(42) Capellos, C.; Benon, H. K. *Kinetic systems*; Wiley-Interscience: New York, 1972.
(43) Rosenthal, S. J.; Xie, X.; Du, M.; Fleming, G. R. *Chem. Phys*. **1991**, *95*, 4715.
(44) Jimenez, R., Fleming, G. R., Kumer, P. V.; Maroncelli, M. *Nature* **1994**, *369*, 471.
(45) Fraser, R. D. B.; Suzuki, E. In *Spectral Analysis*; Blackburn. J. A., Ed.; Marcel Dekker: New York, 1970; p 171.
(46) Pines, E.; Pines, D.; Ma. Y−Z.; Fleming, G. R. *Chem. Phys. Chem.* **2004**, *111*, 111.
(47) Cohen, B.; Leiderman, P.; Huppert, D. *J. Luminescence* **2003**, *102*, 676.
(48) Genosar, L.; Cohen, B.; Huppert, D. *J. Phys. Chem. A* **2000**, *104*, 6689.